Available online at www.sciencedirect.com
SCIENCE DIRECT®
Journal of Solid State Chemistry 177 (2004) 2933–2942
JOURNAL OF SOLID STATE CHEMISTRY
http://elsevier.com/locate/jssc

Phase equilibria in the pseudo-binary system $SrO–Fe_2O_3$

Anita Fossdal, Mari-Ann Einarsrud, and Tor Grande*

Department of Materials Technology, Norwegian University of Science and Technology, Sem Saelands vei 12, Trondheim 7491, Norway

Received 2 March 2004; received in revised form 6 May 2004; accepted 8 May 2004

Abstract

The phase relations in the pseudo-binary system $SrO–Fe_2O_3$ have been investigated in air up to 1150°C by means of powder X-ray diffraction and thermal analysis. $Sr_3Fe_2O_{7-\delta}$, $SrFeO_{3-\delta}$ and $SrFe_{12}O_{19}$ are stable phases in the entire investigated temperature region, whereas $Sr_2FeO_{4-\delta}$ and $Sr_4Fe_3O_{10-\delta}$ decompose above 930 ± 10°C and 850 ± 25°C, respectively. $Sr_4Fe_6O_{13\pm\delta}$ is entropy-stabilized relative to $SrFeO_{3-\delta}$ and $SrFe_{12}O_{19}$ above 775 ± 25°C. Extended solid-solution $Sr_{1\pm x}FeO_{3-\delta}$ was demonstrated. On the Fe-deficient side, the extent of solid solubility appeared to decrease gradually with temperature, whereas an abrupt decrease due to formation of $Sr_4Fe_6O_{13\pm\delta}$ was observed above 775°C on the Sr-deficient side.

Keywords: Phase diagram; Solid solution; $SrO–Fe_2O_3$; Stability

1. Introduction

Complex oxides with iron in the +IV state are rarely found because of the oxidizing conditions needed to prepare them. Despite these problems tetravalent iron is found in several intermediate phases in the pseudo-binary system $SrO–Fe_2O_3$. Batti [1] investigated the pseudo-binary system $SrO–Fe_2O_3$ in oxygen from 1000°C and into the liquid phase and the intermediate phases $Sr_3Fe_2O_7$, $SrFeO_3$, $Sr_7Fe_{10}O_{22}$ and $SrFe_{12}O_{19}$ were reported. $Sr_7Fe_{10}O_{22}$ has later been shown to be $Sr_4Fe_6O_{13+\delta}$ [2], which is unstable at low temperatures [3,4]. Brisi and Rolando [5] later reported the existence of two additional intermediate phases, $Sr_2FeO_{4-\delta}$, and $Sr_4Fe_3O_{10-\delta}$, but these two phases were observed to be unstable at high temperatures. Batti reported that some regions of solid solubility were present in the system [1]. Recently, extended solid solution $Sr_{1\pm x}FeO_{3-\delta}$ was reported by Kleveland et al. [4].

The crystal structures of the intermediate phases in the pseudo-binary system $SrO–Fe_2O_3$ are well known. The Ruddlesden–Popper (RP) type compounds $Sr_{n+1}Fe_nO_{3n+1}$ ($n=1, 2, 3, \infty$) crystallize in structures related to K_2NiF_4 [5–7]. Their crystal structures can be explained by interlayers of SrO (NaCl type) and $SrFeO_{3-\delta}$ (perovskite type) slabs. $Sr_4Fe_6O_{13+\delta}$ has an orthorhombic crystal structure with alternating layers of corner-sharing FeO_6 octahedra and double layers of FeO_5 with Fe in trigonal bipyramidal or square pyramidal coordination polyhedra [2]. $SrFe_{12}O_{19}$ has the magnetoplumbite structure. The crystal structure of $SrFeO_{3-\delta}$ has been investigated as a function of temperature and partial pressure of oxygen by Takeda et al. [8] and Mizusaki et al. [9] Several oxygen vacancy ordered structures with the general formula $Sr_nFe_nO_{3n-1}$ ($n=2$, 4, 8 and ∞) exist in this system. The crystal structures of the vacancy-ordered perovskite phases have recently been reexamined by Hodges et al. [10] (see Ref. [10] for an extensive review of the structural properties of $SrFeO_{3-\delta}$). The vacancy ordered phases consist of alternating layers of FeO_6 octahedra and FeO_5 square pyramids. At low temperatures the crystal structure changes from the cubic perovskite ($\delta\approx0$) via tetragonal ($\delta\approx0.125$) and orthorhombic ($\delta\approx0.25$) perovskites to the orthorhombic brownmillerite structure ($\delta\approx0.5$). Two-phase mixtures are formed between these values of δ. The order–disorder temperature of orthorhombic $SrFeO_{2.725-2.75}$ appears to be influenced by sample preparation, as it has been reported in a

*Corresponding author. Fax: +47-73-59-08-60.
E-mail address: tor.grande@material.ntnu.no (T. Grande).

0022-4596/$ - see front matter © 2004 Elsevier Inc. All rights reserved.
doi:10.1016/j.jssc.2004.05.007

relatively wide temperature range. Takeda et al. [8] measured this transition at 325°C by DTA, whereas Haavik et al. [11] and Fournes et al. [12] measured phase transition temperatures of 387°C and 397°C, respectively. The discrepancy between the reported disordering temperatures for the tetragonal $SrFeO_{2.82-2.86}$ is smaller, the reported values being 250°C [8], 287°C [11] and 297°C [12]. Corresponding oxygen vacancy order–disorder phase transitions in the RP phases has not been reported.

The aim of this study is to re-examine the phase diagram of the pseudo-binary system SrO–Fe_2O_3. The stability of the phases $Sr_2FeO_{4-\delta}$, $Sr_4Fe_3O_{10-\delta}$ and $Sr_4Fe_6O_{13\pm\delta}$ at elevated temperatures was investigated. Moreover, the temperature dependence of the solid solubility $Sr_{1\pm x}FeO_{3-\delta}$ was examined. The stability trend in the $Sr_{n+1}Fe_nO_{3n+1}$ series is addressed. The present findings are summarized in a pseudo-binary phase diagram for the SrO–Fe_2O_3 system.

2. Experimental

2.1. Synthesis

Seven samples in the composition range 20–48.1 mol% Fe_2O_3 were prepared by the solid-state reaction method by mixing stoichiometric amounts of $Sr(NO_3)_2$ (Merck, >99.0 wt%) and Fe_2O_3 (Merck, >99.0 wt%). $Sr(NO_3)_2$ was dried overnight at 300°C prior to use, and thermal analysis showed the nitrate was stoichiometric after the heat treatment. Fe_2O_3 was dried overnight at 1000°C before weighing in the amounts needed for synthesis. Appropriate amounts of the starting materials were mixed and homogenized in a boron carbide mortar. All mixtures were uniaxially pressed into cylindrical samples and annealed in air at 1150°C for 72 h with two intermittent grindings. The heating and cooling rates were 200°C/h. $Sr_2FeO_{4-\delta}$ was prepared by the same method, but by annealing at 750°C in a flowing O_2 atmosphere for 92 h. A heating rate of 20°C/h was used.

$Sr_4Fe_3O_{10-\delta}$ was not successfully synthesized by using $Sr(NO_3)_2$. Near single-phase $Sr_4Fe_3O_{10-\delta}$ was however obtained by using mixtures of $SrCO_3$ (BDH, ⩾98.5 wt%) and Fe_2O_3 annealed for 60 h at 800°C. $SrCO_3$ was dried overnight at 500°C prior to use.

As synthesis of $Sr_2FeO_{4-\delta}$ and $Sr_4Fe_3O_{10-\delta}$ proved to be difficult, attempts were also made to synthesize these compounds at different temperatures and by a modified glycine-nitrate method. This synthesis method is described in detail elsewhere [13].

$SrFeO_{3-\delta}$ powders with variable nominal cation stoichiometry (Sr:Fe = 0.95, ~1, 1.05) were prepared by spray drying (Mini Spray-drier B-191, BÜCHI) of a solution of nitrates and acetates or by spray pyrolysis from glycine-nitrate solutions. Details of the synthesis are given elsewhere [4]. The sample with Sr:Fe = ~1 has been shown to be Sr-deficient [4], but will be referred to by the nominal composition in the following. Extensive Sr or Fe deficient materials relative to the perovskite composition were prepared by solid-state synthesis at 1150°C. As the exact Sr:Fe ratio of the perovskite phase in these materials was difficult to determine exactly due to the solid solution, these materials are termed Sr- and Fe-deficient, respectively. The Fe-deficient material contained $Sr_3Fe_2O_{7-\delta}$ as a secondary phase, whereas the Sr-deficient material contained small amounts of $Sr_4Fe_6O_{13\pm\delta}$ (qualitative powder X-ray diffraction).

$Sr_4Fe_6O_{13\pm\delta}$ powder was prepared by the EDTA (EthyleneDiamineTetraAcetate) precursor method (EDTA). Details of the synthesis are given elsewhere [3].

2.2. Characterization

Powder X-ray diffraction and in situ high-temperature X-ray diffraction (HTXRD) were performed in the 2θ range 5–70° with a Siemens D5005 $\theta-\theta$ diffractometer using Cu$K\alpha$ radiation, a secondary monochromator and a scintillation detector. The HTXRD powder samples were dispersed in isopropanol and the suspension was applied on a Pt strip located in a high temperature camera (HTK 16, Anton Paar GmbH) resulting in a thin layer of the sample on the Pt-strip. The Pt strip was heated to the pre-set temperatures (30–1000°C) by ohmic resistance heating. The temperature was measured by a Pt–Pt10%Rh thermocouple, which was welded to the Pt strip. All measurements were performed in flowing "synthetic" air (99.99%). Prior to each scan, the sample film was held for 30 min at temperature to establish equilibrium. The data were collected with a step size of 0.04° and a count time of 10 s per step. The Pt strip was used as an internal standard in order to determine the unit cell parameters. Due to the multi-phase nature of the samples (described below), only two reflections, (002) and (101) for $Sr_2FeO_{4-\delta}$ and (004) and (101) for $Sr_4Fe_3O_{10-\delta}$, were used in the cell parameter calculations.

Simultaneous thermogravimetric analysis (TG) and differential thermal analysis (DTA) were performed in air on $Sr_2FeO_{4-\delta}$, $Sr_3Fe_2O_{7-\delta}$ and $Sr_4Fe_3O_{10-\delta}$ up to 1000°C with a Netzsch STA 449C (accuracy ±0.5°C, ±0.5 μg) with a heating and cooling rate of 2°C/min. Measurements in N_2 atmosphere ($pO_2 = 5\times10^{-3}$ atm) were performed on $Sr_2FeO_{4-\delta}$ and $Sr_4Fe_3O_{10-\delta}$. The average oxidation state of Fe in $Sr_3Fe_2O_{7-\delta}$ was determined by measuring the dynamic weight loss in air up to 1000°C. The room temperature composition of $Sr_3Fe_2O_{6.75}$ reported by Prado et al. [14] was adopted. Temperature was calibrated using the melting points of Sn, Zn, CsCl, Al and Au.

The average oxidation state of iron in the perovskite materials was determined by TG (Perkin Elmer TGS2) and iodometric titration. The weight change in synthetic air from room temperature to 700°C and from 700°C to 1000°C in steps of 50°C was recorded. The measurements were corrected for changes in buoyancy with temperature and the corrected weight changes were combined with the oxygen stoichiometry obtained by iodometric titration to calculate the average oxidation state of Fe at the different temperatures. In the iodometric titrations, the sample (20–30 mg) was mixed with KI (0.4–0.6 g) and deionized and degassed distilled water (10 mL) in a round-necked vessel. The vessel was flushed with N_2 gas to avoid air-oxidation of excess I^-. Concentrated hydrochloric acid (25 mL) was added to dissolve the sample and the solution was titrated against a 0.01 M sodium thiosulfate solution, using starch as an indicator.

Differential scanning calorimetry (Perkin-Elmer DSC-7) was performed in synthetic air on single-phase $Sr_{1\pm x}FeO_{3-\delta}$ powders and on the Sr- and Fe-deficient materials. The sintered samples were crushed to powders and loaded into Al-capsules. Before the DSC measurement the Al-capsule with the samples were heated to 400°C and then cooled to room temperature in situ to ensure a homogeneous oxygen stoichiometry and to remove adsorbed moisture. Heating and cooling rate was 10°C/min. Measurements were made with a second cycle of the same temperature program. The DSC was calibrated using the melting point of pure In and Zn.

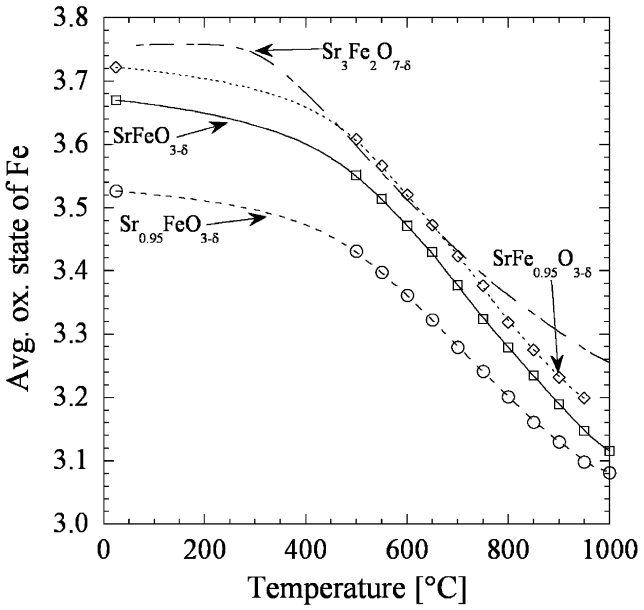

Fig. 1. Average oxidation state of Fe in $Sr_3Fe_2O_{7-\delta}$ and $Sr_{1\pm0.0.05}Fe_{3-\delta}$ as a function of temperature in air.

Table 1
Decomposition temperature of $Sr_2FeO_{4-\delta}$ and $Sr_4Fe_3O_{10-\delta}$ in air and N_2 ($pO_2 = 5\times10^{-3}$ atm)

Composition	Decomposition temperature (°C)	
	Air	N_2 ($pO_2 \sim 10^{-3}$ atm)
$Sr_2FeO_{4-\delta}$	930±10	860±10
$Sr_4Fe_3O_{10-\delta}$	850±25	830±10

3. Results

3.1. Ruddlesden–Popper (RP) type phases

$Sr_3Fe_2O_{7-\delta}$ is stable up to the peritectic melting point (in pure O_2) at ~1520°C [1]. DTA and TG measurements showed no phase transitions in air below 1000°C. The average oxidation state of Fe in $Sr_3Fe_2O_{7-\delta}$ is given as a function of temperature in Fig. 1. The error in the measurements was less than 1%. The average oxidation state of Fe in $Sr_3Fe_2O_{7-\delta}$ is 3.75 at 1000°C, corresponding to the stoichiometry $Sr_3Fe_2O_{6.75}$.

Preparation of phase pure $Sr_2FeO_{4-\delta}$ and $Sr_4Fe_3O_{10-\delta}$ was not successful, which is rationalized by their instability at high temperature and by the high stability of $SrCO_3$ in air. In addition, $Sr_2FeO_{4-\delta}$ reacted relatively fast with atmospheric humidity, even when stored in a desicator, forming $Sr(OH)_2\cdot xH_2O$ and $Sr_3Fe_2O_{7-\delta}$ (confirmed by XRD). The (hydrated) hydroxide was further observed to decompose upon heating, followed by reaction with atmospheric CO_2 to form $SrCO_3$. However, for the study of decomposition reactions, the presence of these secondary phases (see Fig. 3) is not expected to have a significant influence since the solid-state reactions between these phases were observed to be slow in the actual temperature region.

The thermal stability of $Sr_2FeO_{4-\delta}$ and $Sr_4Fe_3O_{10-\delta}$ were studied by both careful DTA/TG and HTXRD analysis. The decomposition temperatures of $Sr_2FeO_{4-\delta}$ and $Sr_4Fe_3O_{10-\delta}$ in air and N_2 ($pO_2 = 5\times10^{-3}$ atm) atmosphere, measured by DTA, are given in Table 1. $Sr_2FeO_{4-\delta}$ decomposes at higher temperatures than $Sr_4Fe_3O_{10-\delta}$ in both air and nitrogen atmosphere. Decreasing the oxygen partial pressure severely lowers the decomposition temperature of $Sr_2FeO_{4-\delta}$, whereas the decomposition of $Sr_4Fe_3O_{10-\delta}$ is less influenced by changes in pO_2. The endothermic peak associated with the decomposition exhibits a sluggish onset, resulting in high uncertainties of the decomposition temperatures. Moreover, the baseline of the DTA instrument was non-linear in this temperature region, adding to the uncertainty. Evolution of oxygen is involved in the decomposition reactions, as demonstrated by the thermogravimetric measurements shown in Fig. 2. Completion of the decomposition is evident by a change in the rate of the oxygen loss. Complete decomposition of $Sr_2FeO_{4-\delta}$ and $Sr_4Fe_3O_{10-\delta}$ was confirmed by XRD

after the thermal analysis measurements. The oxygen non-stoichiometry as a function of temperature could not be determined from the TG data for $Sr_2FeO_{4-\delta}$ and $Sr_4Fe_3O_{10-\delta}$ due to the presence of secondary phases. The $SrCO_3$ impurities were observed to decompose to SrO both in the TG/DTA (350–450°C) and HTXRD (700–800°C) measurements. The discrepancy between the decomposition temperatures is due to different partial pressures of CO_2, as caused by a lower atmosphere exchange rate in the HTXRD camera.

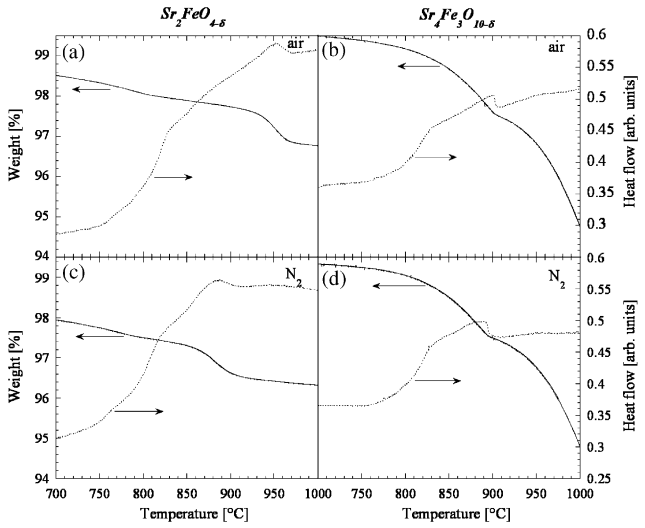

Fig. 2. TG and DTA measurements of (a) $Sr_2FeO_{4-\delta}$ in air, (b) $Sr_4Fe_3O_{10-\delta}$ in air, (c) $Sr_2FeO_{4-\delta}$ in N_2 ($pO_2 \sim 10^{-3}$ atm) and (d) $Sr_4Fe_3O_{10-\delta}$ in N_2 ($pO_2 \sim 10^{-3}$ atm). The heating rate is 2°C/min. The $Sr_2FeO_{4-\delta}$ sample contained $Sr(OH)_2$ and $Sr_3Fe_2O_{7-\delta}$ as secondary phases at room temperature whereas the $Sr_4Fe_3O_{10-\delta}$ sample contained traces of $SrCO_3$ and perovskite.

Selected high-temperature X-ray diffractograms are shown for $Sr_2FeO_{4-\delta}$ in Fig. 3a and for $Sr_4Fe_3O_{10-\delta}$ in Fig. 3b. The initial room temperature phase composition is retained up to 800°C for both samples, with the exception of decomposition of the impurity phase $SrCO_3$. At 900°C, partial decomposition of both $Sr_2FeO_{4-\delta}$ and $Sr_4Fe_3O_{10-\delta}$ is evident and at 1000°C, only minor amounts of $Sr_2FeO_{4-\delta}$ and $Sr_4Fe_3O_{10-\delta}$ remain. The higher apparent decomposition temperatures relative to those measured by thermal analysis may be caused by a temperature gradient in the HTXRD sample due to heat radiation. Above 800°C several diffraction peaks (labeled * in Figs. 3a and b) appear in the high-temperature diffractograms of both the $Sr_2FeO_{4-\delta}$ and $Sr_4Fe_3O_{10-\delta}$ compositions, the intensity increases with increasing temperature. These peaks could not be indexed to a known phase in the SrO–Fe_2O_3 system, hence further investigations are necessary to determine their origin.

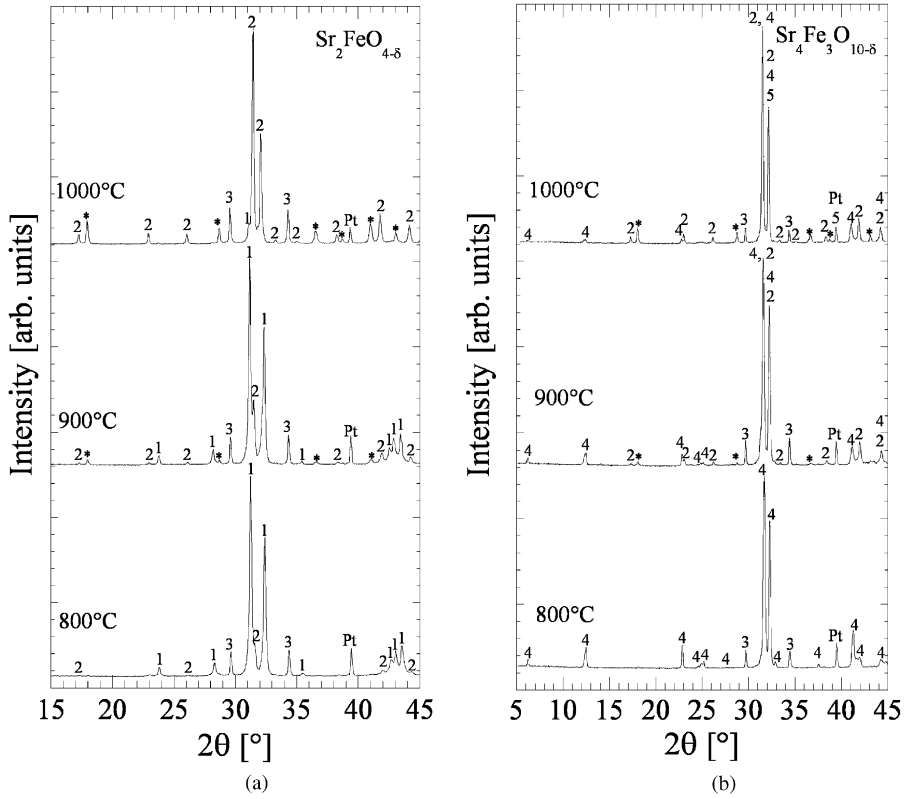

Fig. 3. High-temperature X-ray diffractograms of $Sr_2FeO_{4-\delta}$ (a) and $Sr_4Fe_3O_{10-\delta}$ (b) at 800°C, 900°C and 1000°C. Diffraction lines are labeled according to: 1 = $Sr_2FeO_{4-\delta}$, 2 = $Sr_3Fe_2O_{7-\delta}$, 3 = SrO, 4 = $Sr_4Fe_3O_{10-\delta}$, 5 = $SrFeO_{3-\delta}$ and * = unknown. $Sr(OH)_2$ and $Sr_3Fe_2O_{7-\delta}$ were present as secondary phases at room temperature in $Sr_2FeO_{4-\delta}$, whereas $SrCO_3$ and perovskite were present as secondary phases in $Sr_4Fe_3O_{10-\delta}$ at room temperature. The Pt reflection is due to the heating strip in the furnace.

Combining the present investigations, the RP phases $Sr_2FeO_{4-\delta}$ and $Sr_4Fe_3O_{10-\delta}$ decompose at high temperatures according to the two reactions

$$2Sr_2FeO_{4-\delta_1}\ (s) \rightarrow Sr_3Fe_2O_{7-\delta_2}\ (s) + SrO\ (s) + \left(\frac{\delta_2 - 2\delta_1}{2}\right)O_2\ (g), \quad (1)$$

$$Sr_4Fe_3O_{10-\delta_3}\ (s) \rightarrow Sr_3Fe_2O_{7-\delta_4}\ (s) + SrFeO_{3-\delta_5}\ (s) + \left(\frac{\delta_4 + \delta_5 - \delta_3}{2}\right)O_2\ (g). \quad (2)$$

The unit cell parameters of $Sr_2FeO_{4-\delta}$ and $Sr_4Fe_3O_{10-\delta}$ in air are given as a function of temperature in Fig. 4. Note that unit cell parameters are given also above the decomposition temperature, as the decomposition reactions were incomplete at 1000°C. In both phases the lattice parameter a has a linear dependency on temperature, whereas c are clearly non-linear with temperature. The non-linear behavior of c is characteristic of the chemical expansion associated with thermal reduction of the tetravalent iron to the larger trivalent iron. The reduction is accompanied by an increasing concentration of oxygen vacancies, and the non-linear expansion for only the c-parameter may suggest that oxygen vacancies are mainly formed on the oxygen sites linking the FeO_6 octahedra in the c-direction.

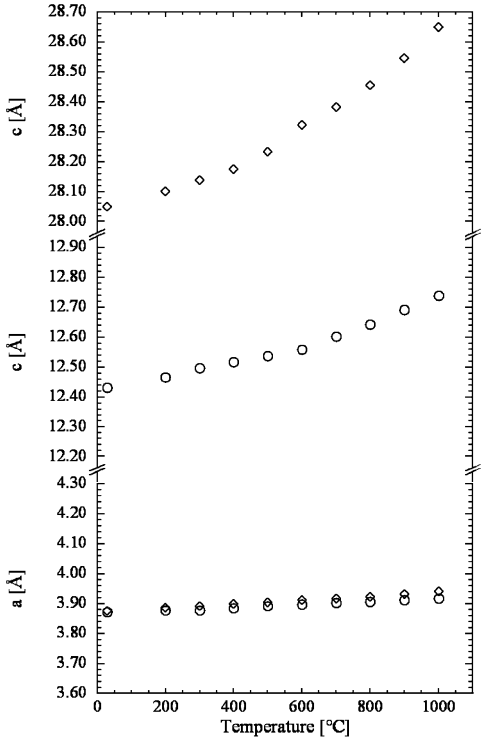

Fig. 4. Unit cell parameters of $Sr_2FeO_{4-\delta}$ (○) and $Sr_4Fe_3O_{10-\delta}$ (◇) in air as a function of temperature. The uncertainties are within the size of the symbols.

The thermal expansion coefficients of both phases were anisotropic. In $Sr_2FeO_{4-\delta}$ the thermal expansion coefficients in the a and c directions were 13×10^{-6} and $18–36 \times 10^{-6}\,K^{-1}$, respectively, whereas the a and c directions in $Sr_4Fe_3O_{10-\delta}$ exhibited thermal expansion coefficients of 17×10^{-6} and $13–36 \times 10^{-6}\,K^{-1}$, respectively. The unit cell parameters of $Sr_2FeO_{4-\delta}$ and $Sr_4Fe_3O_{10-\delta}$ at room temperature are slightly larger than those reported in literature [5,6]. The difference is reasonable, as the current materials were more oxygen deficient than those previously reported.

3.2. Perovskite

$Sr_{1\pm x}FeO_{3-\delta}$ ($x = -0.05,\ 0,\ +0.05$) appeared as single-phase materials or as mixtures of orthorhombic and tetragonal $SrFeO_{3-\delta}$ after calcination at 750°C, according to XRD. Thermogravimetric analysis and iodometric titration measurements of these materials show that the average oxidation state of iron increases with increasing Sr-content in the perovskite. The oxidation state of iron for the three materials is shown in Fig. 1. The room-temperature oxidation states of Fe correspond to $Sr_{0.95}FeO_{2.71}$, $SrFeO_{2.84}$ and $SrFe_{0.95}O_{2.77}$.

In order to investigate the solid solution $Sr_{1\pm x}FeO_{3-\delta}$ it was decided to measure the influence of cation stoichiometry on the phase transitions from the low-temperature vacancy-ordered states to the disordered cubic perovskite. The DSC analyses in air on the $Sr_{1\pm x}FeO_{3-\delta}$ materials are summarized in Fig. 5. All three powders were single-phase perovskite within the detection limits of X-ray diffraction also after DSC measurements. Interestingly, $Sr_{0.95}FeO_{3-\delta}$ and $SrFeO_{3-\delta}$, calcined at 750°C, showed no phase transitions below 400°C, whereas after calcination at 800°C both materials exhibit two overlapping thermal events. The two-phase transitions are interpreted as the tetragonal to cubic (lower temperature) and the orthorhombic to cubic transitions (higher temperature), respectively, in line with previous reports [6,9,10]. The DSC measurements on materials annealed at 1150°C are shown in Fig. 6. A single phase transition was observed in these materials below 400°C, interpreted as the disordering of the orthorhombic vacancy-ordered phase. The phase transition temperatures (Table 2) increase with increasing Sr-content and were measured 2–40°C higher on cooling than on heating, the differences decreasing with increasing Sr-content.

3.3. $Sr_4Fe_6O_{13\pm\delta}$

Calcination of the material with nominal composition $Sr_4Fe_6O_{13\pm\delta}$ below 775°C in air resulted in a mixture of $Sr_{1-x}FeO_{3-\delta}$ and $SrFe_{12}O_{19}$. The $Sr_4Fe_6O_{13\pm\delta}$ phase was only formed when the powder was calcined above

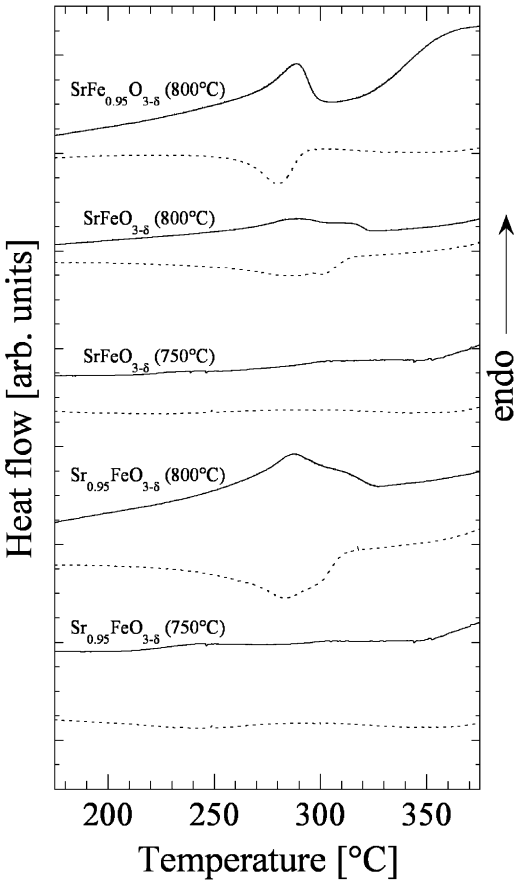

Fig. 5. DSC measurements of $Sr_{0.95}FeO_{3-\delta}$ (calcined at 750°C or 800°C) $SrFeO_{3-\delta}$ (calcined at 750°C or 800°C) and $SrFe_{0.95}FeO_{3-\delta}$ (calcined at 800°C) in air. The solid and broken lines are measured upon heating and cooling, respectively. Heating and cooling rates are 10°C/min.

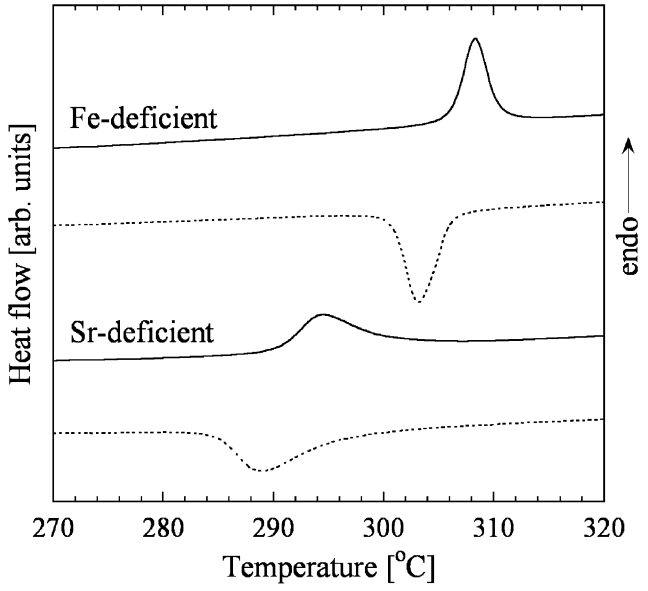

Fig. 6. DSC measurements of Sr-deficient and Fe-deficient $SrFeO_{3-\delta}$ sintered at 1150°C. The solid and broken lines are measured upon heating and cooling, respectively. Heating and cooling rates are 10°C/min.

775°C. The transformation to $Sr_4Fe_6O_{13\pm\delta}$ was slow, and traces of the two parent phases were present even after 120 h firing at 800°C. $Sr_4Fe_6O_{13\pm\delta}$ is entropy stabilized relative to $SrFeO_{3-\delta}$ and $SrFe_{12}O_{19}$ according to the phase equilibrium

$$21SrFeO_{3-\delta_6}\,(s) + SrFe_{12}O_{19}\,(s) \rightarrow \tfrac{33}{6}Sr_4Fe_6O_{13\pm\delta_7}\,(s) + \left(\frac{63\mp 33\delta_7 - 126\delta_6}{12}\right)O_2\,(g). \quad (3)$$

Solid solubility in the perovskite phase is omitted in reaction (3) for simplicity.

$Sr_4Fe_6O_{13}$ was not observed to oxidize to $Sr_{1-x}FeO_{3-\delta}$ (and $SrFe_{12}O_{19}$) during cooling, hence metastable $Sr_4Fe_6O_{13}$ was retained below 775°C.

3.4. The pseudo-binary SrO–Fe_2O_3 system

The existence of all the phases above 1000°C previously reported by Batti [1] was confirmed by XRD analysis on samples with composition in the range 20–48.1 mol% Fe_2O_3. The actual composition of the phase $7SrO \cdot 5Fe_2O_3$ is confirmed to be $Sr_4Fe_6O_{13\pm\delta}$. The observed phases along the composition line SrO–Fe_2O_3 below 1150°C in air are summarized in the pseudo-binary phase diagram shown in Fig. 7.

4. Discussion

4.1. Ruddlesden–Popper type phases

Whereas $SrFeO_{3-\delta}$ ($n = \infty$) and $Sr_3Fe_2O_{7-\delta}$ ($n = 2$) are stable at high temperatures, the $n = 1$ and 3 members of the RP class of compounds decompose at elevated temperatures. The reason for this difference in stability is not obvious, but the ability to tolerate extensive concentration of oxygen vacancies is likely to be an important factor.

The formation reaction of oxygen stoichiometric RP phases can be written as

$$(n+1)SrO + (n/2)Fe_2O_3 + n/4O_2 \rightarrow Sr_{n+1}Fe_nO_{3n+1}. \quad (4)$$

At low temperatures, the $Sr_{n+1}Fe_nO_{3n+1}$ phases are stable for $n = 1$, 2, 3 and ∞. The enthalpy of formation from the binary oxides, reaction (4), has been reported for $n = 2$ and ∞ by Massazza and Fadda [15]. The enthalpy of formation of $Sr_3Fe_2O_{7-\delta}$ (−54.2 kJ/mol cation) is significantly more exothermic than for $SrFeO_{3-\delta}$ (−32.3 kJ/mol cation). Although the oxygen deficiencies of these samples were not determined, these data demonstrate that the enthalpy of formation decreases with increasing SrO content and that

Table 2
Phase transition temperatures for $Sr_{1\pm x}FeO_{3-\delta}$ materials in air. T→C denotes the tetragonal to cubic and O→C the orthorhombic to cubic phase transition, respectively

Composition	Calc./firing temperature (°C)	Heating		Cooling	
		T→C (°C)	O→C (°C)	T→C (°C)	O→C (°C)
$Sr_{0.95}FeO_{3-\delta}$	800	260±5	285±5	300±5	312±5
$SrFeO_{3-\delta}$	800	266±5	285±5	303±5	314±5
$SrFe_{0.95}O_{3-\delta}$	800	270±5	—	294±5	—
Sr-deficient	1150	—	290±2	—	298±2
Fe-deficient	1150	—	306±2	—	308±2

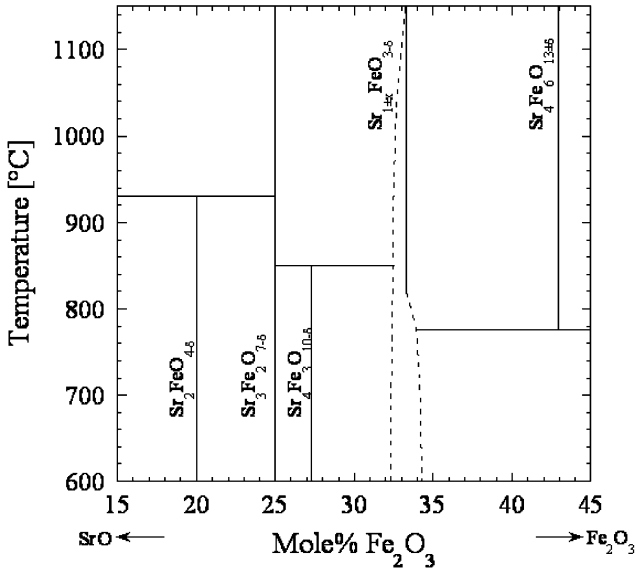

Fig. 7. Low-temperature section of the pseudo-binary phase diagram in the SrO–Fe_2O_3 system in air.

energetically the most stable phases are at a high concentration of the basic oxide SrO.

At elevated temperatures, reduction of tetravalent iron to trivalent iron and the corresponding creation of oxygen vacancies occur according to the reaction

$$Sr_{n+1}Fe_nO_{3n+1} \rightarrow Sr_{n+1}Fe_nO_{3n+1-\delta} + \delta/2O_2\,(g). \quad (5)$$

For $\delta = n/2$, all Fe is reduced to the trivalent state.

As a first approximation, reaction (5) can be represented by the point defect equilibrium

$$2Fe_{Fe}^{x} + O_O^x = 2Fe_{Fe}' + V_O^{\bullet\bullet} + \tfrac{1}{2}O_2\,(g), \quad (6)$$

where O_O^x is oxygen on an oxygen site, $V_O^{\bullet\bullet}$ is a vacancy on an oxygen site, Fe_{Fe}^x is tetravalent Fe on a Fe site and Fe_{Fe}' is trivalent Fe on a Fe site. Here it is assumed that there are no interactions between the point defects and that defect ordering does not occur. Haavik et al. [16] have shown that the oxygen non-stoichiometry of $SrFeO_{3-\delta}$ is reasonably described by such a simple approach. The point defect reaction is characterized by a large endothermic enthalpy and a large positive entropy due to the formation of O_2(g). The contribution to the Gibbs energy of formation (from their binary oxides) is in fact in the same order of magnitude as the enthalpy of reaction (4) for $SrFeO_{3-\delta}$. It is therefore clear that reaction (5) could possibly govern the relative stability of the RP phases.

Our findings demonstrate that the $n = 1$ and 3 phases are destabilized relative to $n = 2$, due to the reduction of the valence state of Fe and formation of oxygen vacancies as described by the simple point defect equilibrium (6). Here it is interesting to note that the $n = 1$ and 3 phases contain an odd number of perovskite layers, while the $n = 2$ phase contains an even number of perovskite layers. The energetics of oxygen vacancies in the perovskite layers and at the interface between the SrO and perovskite layers in RP phases seems therefore to be different. The energetics of the formation of oxygen vacancies may therefore depend strongly upon which of the lattice sites that become vacant in the RP phases. For $n = 2$ the perovksite double layer allows ordering of the oxygen vacancies by total removal of the oxygen linking the octahedral layers [7]. The stronger pO_2 dependence of the decomposition of $Sr_2FeO_{4-\delta}$ relative to $Sr_4Fe_3O_{10-\delta}$ supports this suggestion. The low decomposition temperature observed for $n = 1$ and 3 indicates that the energetics of the point defect are less favorable for these compounds and that only $Sr_3Fe_2O_{7-\delta}$ and $SrFeO_{3-\delta}$ can tolerate high oxygen vacancy concentrations. The compounds $Sr_2Fe_2O_5$ and $Sr_3Fe_2O_6$, where Fe is formally in the trivalent state, are indeed stable at reduced oxygen pressures at high temperatures [7,9], whereas the ability of $Sr_2FeO_{4-\delta}$ and $Sr_4Fe_3O_{10-\delta}$ to tolerate oxygen non-stoichiometry under ambient or reduced oxygen pressures has not been reported. Single-phase $Sr_2FeO_{3.7}$ has however been observed at 1007°C under a pO_2 of 190.5 atm [17].

The decomposition of $Sr_2FeO_{4-\delta}$ and $Sr_4Fe_3O_{10-\delta}$ is slow, as seen by both thermal analysis and HTXRD. The slow decomposition is in part due to low cation diffusion rates at the decomposition temperatures. As argued above, the differences in thermodynamic quantities between the RP-phases are expected to be small,

hence kinetics largely govern the decomposition reactions. Due to the similarity of the structures, disordered intergrowths between the different phases are expected to form, as seen for the SrO–TiO_2 system [18,19].

Synthesis of the RP-phases $Sr_2FeO_{4-\delta}$ and $Sr_4Fe_3O_{10-\delta}$ by the solid-state reaction method is complicated by low cation diffusion rates below the decomposition temperatures and the stability of $SrCO_3$ at low temperatures. The latter can to some extent be circumvented by using $Sr(NO_3)_2$ rather than $SrCO_3$. $Sr(NO_3)_2$ will first melt, followed by decomposition and formation of SrO. The Sr:Fe ratio after annealing was observed to be lower than the initial ratio when $Sr(NO_3)_2$ was used as a reactant. The proposed explanation for this discrepancy is evaporation of $Sr(NO_3)_2$. The apparent evaporation of a Sr-containing compound has also been observed previously [3]. A slow heating rate was necessary to obtain a controlled decomposition of the nitrate, but slow heating was also observed to increase the apparent evaporation.

The synthesis of $Sr_4Fe_3O_{10-\delta}$ proved to be most challenging. The nucleation and growth of $Sr_4Fe_3O_{10-\delta}$ appears to be sensitive to the homogeneity of the starting powder mixture, as different batches of the same nominal composition could contain different phases after being subjected to the same firing sequence. As an example, firing mixtures of $SrCO_3$ and Fe_2O_3 in stoichiometric amounts at 800°C yielded a mixture of $Sr_3Fe_2O_{7-\delta}$ and SrO in one case, whereas another, similar batch gave close to phase pure $Sr_4Fe_3O_{10-\delta}$ after firing. Attempts to reverse reaction (2) at 700°C were not successful even after two weeks annealing time.

The high temperatures in the combustion step [20] of the glycine-nitrate synthesis were seen to cause the formation of a non-equilibrium mixture of binary and ternary oxides. In case of $Sr_3Fe_2O_{7-\delta}$, a calcination temperature at or above 900°C was sufficient to produce a single-phase material, whereas single-phase $Sr_2FeO_{4-\delta}$ and $Sr_4Fe_3O_{10-\delta}$ could not be obtained by this method due to the slow reversal rate of reactions (1) and (2) at ambient pressures. Reversal of reaction (1) has however previously been obtained by Dann et al. [6] at 750°C under an oxygen pressure of 200 atm.

4.2. $Sr_4Fe_6O_{13\pm\delta}$

The phase $Sr_4Fe_6O_{13}$ is entropy stabilized relative to $SrFe_{12}O_{19}$ and $Sr_{1-x}FeO_{3-\delta}$, as inferred from reaction (3). The reaction is rationalized by the stability of tetravalent Fe in $Sr_{1-x}FeO_{3-\delta}$ at low temperatures. An endothermic enthalpy for reaction (3) is expected due to the high content of tetravalent iron in $Sr_{1-x}FeO_{3-\delta}$ at low temperature and only a moderate content of tetravalent in metastable $Sr_4Fe_6O_{13+\delta}$ at low temperature [21,22].

4.3. Perovskite

The absence of phase transitions in $Sr_{0.95}FeO_{3-\delta}$ and $SrFeO_{3-\delta}$ materials, calcined only at 750°C, implies that the oxygen vacancies are disordered even at low temperatures in these materials. Increasing the calcination temperature to 800°C causes precipitation of entropy-stabilized $Sr_4Fe_6O_{13\pm\delta}$ in these materials, as observed by Kleveland et al. [4]. The solid solubility limit on the Sr-deficient side thus decreases abruptly at this temperature.

Both the tetragonal to cubic and the orthorhombic to cubic phase transition temperatures of $SrFeO_{3-\delta}$ increase with increasing nominal Sr-content in the perovskite, when comparing materials with the same thermal history. The differing phase transition temperatures infers a different Sr:Fe ratio in the $SrFeO_{3-\delta}$ phase. The tetragonal to cubic phase transition temperatures correspond well with the literature values [6,11,12]. The orthorhombic to cubic phase transition temperatures correspond reasonably with the phase transition temperature of 325°C measured by Takeda et al. [6], whereas the phase transition temperatures reported by Haavik et al. [11] and Fournes et al. [12] are considerably higher. The increase in phase transition temperature with nominal Sr-content is likely to be linked with the observation that an increasing Sr-content (or decreasing Fe-content) in the perovskite stabilizes a higher average oxidation state of Fe (Fig. 1).

The apparent solid solubility on either side of the perovskite composition may be due to either solid solution, i.e. cation vacancies on the Sr and Fe sites, or due to disordered intergrowths of the perovskite and the coexistent phase. On the Fe-deficient side, the RP-phases $Sr_4Fe_3O_{10-\delta}$ (at low temperatures) or $Sr_3Fe_2O_{7-\delta}$ (at high temperatures) can be considered as ordered intergrowths between SrO of rock salt structure and perovskite. It is therefore likely that disordered intergrowths between the RP-phases and the perovskite can occur. On the Sr-deficient side, the perovskite phase is coexistent with the magnetoplumbite-type phase $SrFe_{12}O_{19}$ below 775°C. The magnetoplumbite structure is not perovskite-related [23], hence intergrowth between $SrFeO_{3-\delta}$ and $SrFe_{12}O_{19}$ is not expected. Above 775°C, the perovskite-related [2] $Sr_4Fe_6O_{13\pm\delta}$ phase is stabilized. Bredesen et al. [24] have documented nano-scale intergrowths of $La_{1-x}Sr_xFeO_{3-\delta}$ in La-doped $Sr_4Fe_6O_{13\pm\delta}$, which suggests that intergrowth of $SrFeO_{3-\delta}$ and $Sr_4Fe_6O_{13\pm\delta}$ is possible. The oxygen vacancy ordering observed in both Sr- and Fe-deficient perovskites infers ordering of trivalent and tetravalent Fe. We therefore interpret the observed variations in Sr:Fe ratio to reflect solid solution rather than disordered intergrowths.

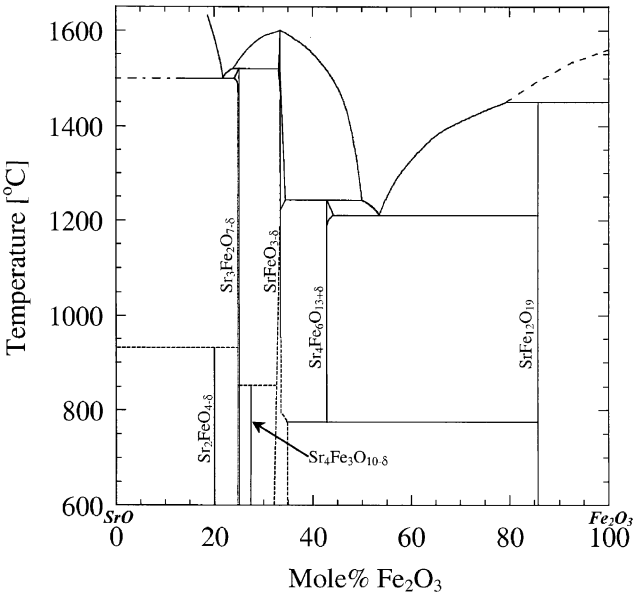

Fig. 8. Pseudo-binary phase diagram in the system SrO–Fe_2O_3 in air. The high-temperature (>1000°C) region was measured in O_2 atmosphere and is redrawn from Batti [1].

4.4. The pseudo-binary SrO–Fe_2O_3 system

According to Gibbs phase rule, the phase equilibria (1), (2) and (3) correspond to invariant points at a constant partial pressure of O_2. As all three reactions involve evolution of oxygen gas, the decomposition temperatures of $Sr_2FeO_{4-\delta}$ and $Sr_4Fe_3O_{10-\delta}$ and the formation temperature of $Sr_4Fe_6O_{13\pm\delta}$ are expected to increase with increasing partial pressure of oxygen.

The SrO–Fe_2O_3 phase diagram reported by Batti [1] is redrawn in Fig. 8, including the present results. The $Sr_7Fe_{10}O_{22}$ phase in the original diagram is redrawn at the correct $Sr_4Fe_6O_{13\pm\delta}$ composition. Observations by Kleveland et al. [4] on the variations of the A:B ratio of $SrFeO_{3-\delta}$ as a function of temperature are also shown. Note that the measurements for the phase diagram constructed by Batti [1] were conducted in a pure O_2 atmosphere. The difference in pO_2 between air and O_2 is here assumed to have minor influence on the high-temperature phase relations in the system since trivalent Fe is expected to be dominant at high T. As an example, the eutectic temperature in air has been measured to 1205 ± 5°C in air [3] as compared to 1210°C in a pure O_2 atmosphere [1].

5. Conclusions

The RP type phases $Sr_2FeO_{4-\delta}$ and $Sr_4Fe_3O_{10-\delta}$ decompose in air at 930 ± 10°C and 850 ± 25°C, respectively. Lowering the partial pressure of oxygen to 5×10^{-3} atm decreased the decomposition temperature by 70°C for $Sr_2FeO_{4-\delta}$ and by 20°C for $Sr_4Fe_3O_{10-\delta}$. No phase transitions were observed below 1000°C in air for RP phases $Sr_{1+n}Fe_nO_{3n+1-\delta}$ with $n=1$, 2, and 3. The variation in the unit cell parameters of $Sr_2FeO_{4-\delta}$ and $Sr_4Fe_3O_{10-\delta}$ with temperature suggests that thermally induced oxygen vacancies are located on sites linking FeO_6 octahedra in the c-direction. The perovskite phase in this system is seen to tolerate deviations in cation stoichiometry, exceeding $Sr_{1\pm0.05}FeO_{3-\delta}$ at low temperatures. On the Fe-deficient side, the extent of solid solubility appears to decrease gradually with temperature, whereas an abrupt decrease at 775°C due to precipitation of $Sr_4Fe_6O_{13\pm\delta}$ is proposed on the Sr-deficient side. $Sr_4Fe_6O_{13\pm\delta}$ is entropy-stabilized relative to $SrFeO_{3-\delta}$ and $SrFe_{12}O_{19}$ above 775 ± 25°C in air.

Acknowledgments

Financial support from the Research Council of Norway and NTNU is acknowledged.

References

[1] P. Batti, Ann. Chim. (Rome) 52 (1962) 941.
[2] A. Yoshiasa, K. Ueno, F. Kanamaru, H. Horiuchi, Mater. Res. Bull. 21 (1986) 175.
[3] A. Fossdal, L.T. Sagdahl, M.-A. Einarsrud, K. Wiik, T. Grande, P.H. Larsen, F.W. Poulsen, Solid State Ionics 143 (2001) 367.
[4] K. Kleveland, M.-A. Einarsrud, T. Grande, J. Am. Ceram. Soc. 83 (2000) 3158.
[5] C. Brisi, P. Rolando, Ann. Chim. (Rome) 59 (1969) 385.
[6] S.E. Dann, M.T. Weller, D.B. Currie, J. Solid State Chem. 92 (1991) 237.
[7] S.E. Dann, M.T. Weller, D.B. Currie, J. Solid State Chem. 97 (1992) 179.
[8] Y. Takeda, K. Kanno, T. Takada, O. Yamamoto, M. Takano, N. Nakayama, Y. Bando, J. Solid State Chem. 63 (1986) 237.
[9] J. Mizusaki, M. Okayasu, S. Yamauchi, K. Fueki, J. Solid State Chem. 99 (1992) 166.
[10] J.P. Hodges, S. Short, J.D. Jorgensen, X. Xiong, B. Dabrowski, S.M. Mini, C.W. Kimball, J. Solid State Chem. 151 (2000) 190.
[11] C. Haavik, T. Atake, H. Kawaji, S. Stølen, Phys. Chem. Chem. Phys. 3 (2001) 3863.
[12] L. Fournes, Y. Potin, J.-C. Grenier, G. Demazeau, M. Pouchard, Solid State Commun. 62 (1987) 239.
[13] A. Fossdal, Dr.ing Thesis, Norwegian University of Science and Technology, Trondheim, Norway, 2003.
[14] F. Prado, T. Armstrong, A. Caneiro, A. Manthiram, J. Electrochem. Soc. 148 (2001) J7.
[15] F. Massazza, R. Fadda, Ann. Chim. (Rome) 54 (1964) 95.
[16] C. Haavik, T. Atake, S. Stølen, Phys. Chem. Chem. Phys. 4 (2002) 1082.
[17] P.K. Gallagher, J.B. MacChesney, D.N.E. Buchanan, J. Chem. Phys. 45 (1966) 2466.
[18] S. Sturm, A. Recnik, C. Scheu, M. Ceh, J. Mater. Res. 15 (2000) 2131.
[19] W. Tian, X.Q. Pan, J.H. Haeni, D.G. Schlom, J. Mater. Res. 16 (2001) 2013.
[20] L.A. Chick, L.R. Pederson, G.D. Maupin, J.L. Bates, L.E. Thomas, G.J. Exarhos, Mater. Lett. 10 (1990) 6.

[21] T. Armstrong, S. Guggilla, A. Manthiram, Mater. Res. Bull. 34 (1999) 837.
[22] F.W. Poulsen, K. Wiik, in: K. Nisancioglu (Ed.), Proceedings of the International Energy Agency Workshop: Materials and Mechanisms, Wadahl, Norway, 1999.
[23] R. Gerber, Z. Simsa, L. Jensovsky, Czech. J. Phys. 44 (1994) 937.
[24] R. Bredesen, T. Norby, A. Bardal, V. Lynum, Solid State Ionics 135 (2000) 687.